Backscattering by a spherical shell close to the air-water interface Comparison experiment / modeling

Jean-Pierre Sessarego[1], Natalie Grigorieva[2], Gregory Fridman[2], and Paul Cristini[1]

[1]CNRS/LMA 31 Chemin Joseph Aiguier, 13402 Marseille cedex 20, France (sessarego@lma.cnrs-mrs.fr)

[2]Department of Applied Mathematics and Mathematical Modeling, St. Petersburg State Marine Technical University, 3 Lotsmanskaya Str. 190008 St. Petersburg, Russia (nsgrig@natalie.spb.su)

When an object is close to a boundary, the interactions between the object and boundary can lead to a very complex structure of the scattered signal masking the free field response of the object. In this work we have studied the backscattered field of a spherical elastic shell close to the air-water interface in the frequency range ($0<k_0a<60$). Numerical simulations are based on a multiple scattering approach.

The experiments were carried out in the laboratory on a thin spherical shell placed beneath the air/water interface. The shell was successively "illuminated" by two wide band transducers working in the frequency range [200 kHz-650 kHz]. This frequency domain was chosen in order to excite resonances associated with both the A_0 and S_0 waves propagating along the shell surface. Free field resonances of the shell were identified in the measured spectrum as well as in the numerical modelling. It was shown that, when the object is close to an interface, in addition to geometrical reflections between the object and the air/water interface, strong interactions due to these resonances could be observed. Experimental results were compared to exact computations for different angles of illumination and different distances of the shell from the air/water interface.

1 Introduction

Acoustic waves scattered from elastic objects immersed in water yield information about the object that can be used for identification. However, when objects are close to the air-water interface or close to the sea bottom, identification becomes much more difficult because of the local effects of the environment. These effects are essentially due to both interactions of the insonifying wave with the air-water interface and object-interface interactions including multiple reflections of the scattered field. This problem was addressed by several authors during the last years [1,2,3,5], but at our knowledge, no studies including modelling in both frequency and time domains for different distances from the object to the interface, varying angles of insonification and different wide band pulses are available. Moreover, if controlled experimental measurements are needed to test the robustness of numerical models, these measurements are practically non existent.

In the present paper we examine in details the backscattering by a spherical elastic shell close to the air-water interface and compare the obtained computational results with the data from a controlled experiment in a water tank.

To make a quantitative comparison with experiments, we used a thin spherical elastic shell of thickness 4% of the outer radius. This shell was filled out with air. The p-wave and s-wave speeds of the elastic material of the shell were obtained from the elastic modulus of the material given by the manufacturer, and density was measured in the laboratory. These values were confirmed by comparing the measured and calculated free field backscattering form functions in water. In order to insonify the shell, two wide band Panametrics transducers working at respectively 250 kHz (bandwidth: 120 kHz at -3dB) and 500 kHz (bandwidth: 250 kHz at -3dB) were used.

Numerical computations of the scattered field were made over a wide frequency range of $0<k_0a<60$ ($k_0=\omega/c_0$, a is the shell radius). This is the range where resonances corresponding both to symmetrical S_0 and antisymmetrical A_0 Lamb waves can be excited on the shell.

2 The solution of the backscattering problem in the frequency domain

The geometry of the problem is shown in Fig. 1. The point source emitting the incident spherical wave is located in water, just beneath the air-water interface, at S(r, θ, 0) in the (r, θ, ϕ) spherical system of coordinates, and S=S (ρ, 0, z) in the cylindrical coordinate system.

The problem of finding the backscattered field taking into account all the interaction effects between the object and air-water interface was examined in many papers. In particular, in Huang and al. [1] the solution was found by the method of images. However, we will use the T-matrix method [2] because it can be generalized to the case of an object near a seabed interface [3].

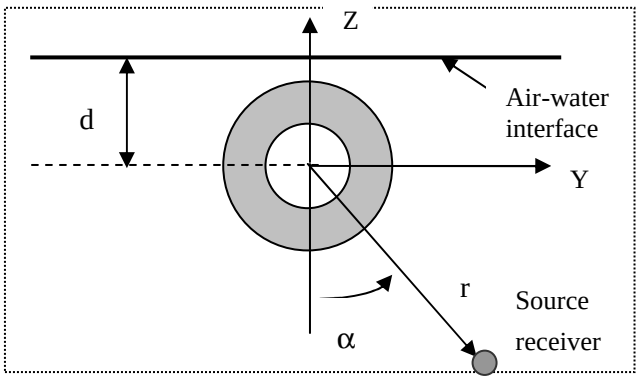

Fig.1. Scattering geometry

In a bounded environment (see Fig.1), the total field observed at point S can be represented in the form [2, 5]

$$\tilde{\Phi}_{total} = \tilde{\Phi}_{source} + \tilde{\Phi}_{scatterer}, \quad (1)$$

where

$$\tilde{\Phi}_{source} = -\frac{e^{2ik_0(d + r\cos\alpha)}}{8\pi(d + r\cos\alpha)} \quad (2)$$

is the spherical wave reflected from the interface, and

$$\tilde{\Phi}_{scatterer} = -\frac{i}{k_0}\sum_{l=0}^{l_{max}}\sum_{m=0}^{l} A_{ml}(\vec{r})T_l\, c_{ml} \quad (3)$$

is the scattered field.

In Eq. (3), T_l are elements of the free-field **T** matrix for the acoustical scattering by a spherical shell. They are written in the form of a ratio of two determinants

$$T_l = \frac{T_l^{(1)}}{T_l^{(0)}}. \quad (4)$$

In the special case of a shell filled with air, $T_l^{(1)}$ and $T_l^{(0)}$ are 6x6 determinants, which are obtained from the boundary conditions at the inner and outer surfaces of the shell. They can be written as

$$T_l^{(1)} = \begin{vmatrix} t_{10} & t_{12} & t_{13} & t_{14} & t_{15} & 0 \\ t_{20} & t_{22} & t_{23} & t_{24} & t_{25} & 0 \\ 0 & t_{32} & t_{33} & t_{34} & t_{35} & 0 \\ 0 & t_{42} & t_{43} & t_{44} & t_{45} & t_{46} \\ 0 & t_{52} & t_{53} & t_{54} & t_{55} & t_{56} \\ 0 & t_{62} & t_{63} & t_{64} & t_{65} & 0 \end{vmatrix}$$

and

$$T_l^{(0)} = \begin{vmatrix} t_{11} & t_{12} & t_{13} & t_{14} & t_{15} & 0 \\ t_{21} & t_{22} & t_{23} & t_{24} & t_{25} & 0 \\ 0 & t_{32} & t_{33} & t_{34} & t_{35} & 0 \\ 0 & t_{42} & t_{43} & t_{44} & t_{45} & t_{46} \\ 0 & t_{52} & t_{53} & t_{54} & t_{55} & t_{56} \\ 0 & t_{62} & t_{63} & t_{64} & t_{65} & 0 \end{vmatrix}.$$

Elements of these determinants are expressed via the spherical Hankel and Bessel functions and their derivatives.

The truncation level l_{max} appearing in Eq.(3) was set by a rule suggested by Kargl and Marston [4] (see, also [5], p.1767)

$$l_{max} = [k_0 a + 4.05(k_0 a)^{1/3}] + 3,$$

where [x] is the integer part of x. The coefficients A_{ml} are given by the following relation:

$$A_{ml}(\bar{r}) = i(\frac{\varepsilon_m}{2\pi})^{1/2}\int_0^\infty \frac{qdq}{h} J_m(q\rho)\left(e^{-ihz}B_{ml}(\frac{h}{k_0}) - e^{ih(2d-z)}B_{ml}(-\frac{h}{k_0})\right). \quad (5)$$

Here ε_0=1, ε_m=2 for $m \geq 1$, and $h = \sqrt{k_0^2 - q^2}$; $\mathrm{Im}(h) \geq 0$, J_m is the cylindrical Bessel function of the m-th order and

$$B_{ml}(\frac{h}{k_0}) = i^{l-m}\left(\frac{2l+1}{2}\frac{(l-m)!}{(l+m)!}\right)^{1/2} P_l^m(\frac{h}{k_0}),$$

P_l^m is the associated Legendre function of order l and rank m.

Equation (5) can be written as the sum of two terms [3]:

$$A_{ml} = A_{ml}^{(f)} + A_{ml}^{(d)}.$$

The first summand is a single outgoing spherical harmonic of the field scattered from a target, written in the form of a plane wave decomposition. The second summand is the wave field resulting from the reflection of the (l, m) spherical harmonic off the air-water interface. It tends to zero as d tends to infinity.

Coefficients c_{ml} in Eq. (3) are found from a linear system of algebraic equations:

$$c_{ml} = A_{ml}(\bar{r}) + i\sum_{l'=m}^{l'_{max}} R_{l,l'}^m T_{l'} c_{ml'}, \quad (6)$$

where $l'_{max} = l_{max}$ and $0 \leq m \leq \min(l, l')$,

$$R_{l,l'}^m = 2i\int_0^\infty \frac{qdq}{hk_0} B_{ml}(-\frac{h}{k_0})B_{ml}(-\frac{h}{k_0})e^{2ihd}. \quad (7)$$

$R^m_{l,l'}$ is the conversion coefficient of the l-th outgoing harmonic into the l'-th incoming harmonic reflected from

the air-water interface. It can be expressed via the Wigner 3j-symbols [3,6,7].

Finding of the coefficients c_{ml} at large k_0a is a very time consuming procedure, because of both the calculation of the Wigner 3j-symbols and the resolution of the system (6). In reality, to find the coefficients c_{ml} it is necessary to solve lmax+1systems of equations: a system of lmax+1 equations with lmax+1 unknowns at m=0, a system of l_{max} equations with l_{max} unknowns at m=1, etc…, and finally a system consisting of one equation with one unknown value $c_{lmaxlmax}$ at m =l_{max}.

3 Comparison experiment/modeling for the free field

In notations used above, the backscattered free field of a spherical shell has the following form:

$$\tilde{\Phi}^{(f)}(\omega) = -\frac{i}{k_0}\sum_{l=0}^{l_{max}}\sum_{m=0}^{l} T_l [A_{ml}^{(f)}(\bar{r})]^2, \qquad (8)$$

where

$$A_{ml}^{(f)} = ik_0 h_l^{(1)}(k_0 r)\xi_{lm} P_l^m(-\cos\alpha). \qquad (9)$$

In Eq. (9), $h_l^{(1)}$ is the spherical Hankel function of the first kind,

$$\xi_{lm} = \left(\frac{\varepsilon_m (2l+1)(l-m)!}{4\pi(l+m)!}\right)^{1/2}. \qquad (10)$$

In order to compute the free field form function, we used the following expression:

$$\left|F^{(f)}(\omega)\right| = \frac{8\pi r^2}{a}\left|\tilde{\Phi}^{(f)}(\omega)\right|, \qquad (11)$$

where r is the distance to the field point and a is the outer radius of the object.

Computations were made for parameters of the spherical shell used in the experiments. This shell was made of an alloy composed of nickel and molybdenum. Physical parameters of this material are given in Table 1. A graph of the free field form function as a function of k_0a is shown in Fig. 2. In this Figure we can observe several different domains. In particular, in the range $20<k_0a<35$ we can see a region of strong high-Q resonances which are directly connected with the well known antisymmetric Lamb wave A_0, and in the range $10<k_0a<20$ resonances related to the symmetric Lamb wave S_0. These resonances have been studied in details by several authors during the last 20 years (see, for example, [8, 9, 10]).

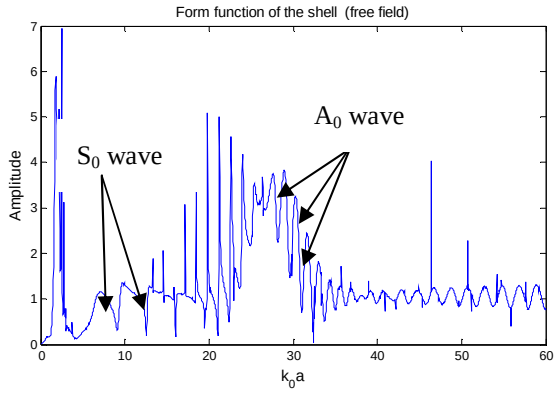

Fig. 2 Form function of a spherical shell as a function of k_0a

P-wave speed	5554.5m/s
S-wave speed	3020.8m/s
Density	9217kg/m^3
Inner radius	1.44 cm
Outer radius	1.5cm

Table I. Physical properties of the shell

3.1 Tank experiments

In order to check our theoretical results, we made a quantitative comparison with an experiment in well controlled conditions. The physical properties of the shell are given in Table 1. The shell was placed just beneath the air-water interface. It was illuminated by two wide band transducers, the first one working at 250 kHz (Bandwidth=120 kHz at -3dB) and the second one at 500 kHz (Bandwidth=250 kHz at -3dB). The echoes were received by the transmitter/receiver system and recorded on a 40MHz A/D card

The carriage supporting the transducer can be moved in the X, Y and Z position with a high degree of accuracy, all the movements being controlled by stepping motors; the angular direction of the transducer itself can be changed by steps of 1/10° between 0° and 180°. This set-up allows a very accurate positioning of the transducer in the tank.

The digitized signals obtained from the experiment could not be used directly for comparison with theoretical curves. To make a comparison in the frequency domain, we first applied the inverse Fourier transform to these signals. The spectrum contains not only the information about target but it includes also the filtering effect of the transducer. In order to compare the theoretical form function with the echo spectrum, we have multiplied the form function by a window W(ω) taking into account the filtering effect of the transducers:

$$\left|F_w^{(f)}(\omega)\right| = \frac{8\pi r^2}{a}\left|\tilde{\Phi}^{(f)}(\omega).W(\omega)\right|. \qquad (12)$$

3.2 Comparison theory-experiment

Figures 3a and 3b give a comparison in the frequency domain for the two different transducers used in the experiment. They show a good agreement between modelling and experiment. Except the very narrow spikes predicted by theory and which cannot be observed in the experiment, all the other resonances can be clearly seen.

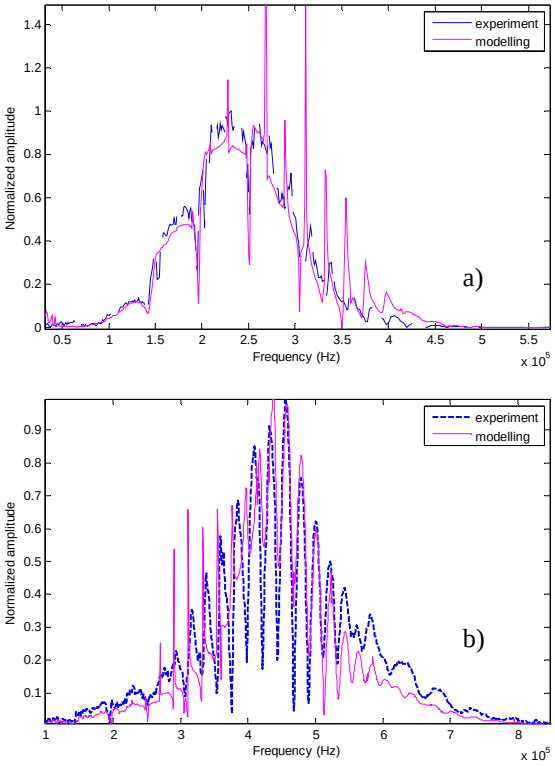

Fig. 3 Comparison of the free field response of the shell: a) transducer T1 (250 kHz); b) transducer T2 (500 kHz)

In the time domain there is a good agreement for both frequencies (250 kHz and 500 kHz). The small differences observed on the amplitudes of signals are certainly due to some imperfection in the manufacturing of the shell, in particular in the welding of the two hemispherical caps. In the upper curve of Fig. 4 we can observe different components which correspond to surface waves of the S_0 type. In the lower curve, surface waves of the A_0 type are clearly seen. They are dispersive as it is predicted by the theory and they appear in the echo with a repetition rate corresponding to a circumnavigation around the shell. These waves are supersonic. Their sound speeds were measured in [11]. The value obtained for the group velocity was: Cg=1890m/s for k_0a~20. In the case of the symmetrical wave S_0 the value obtained for the group velocity was: Cg=5000m/s for k_0a~20. For comparison between experiment and calculation the distance r between the source and object (see Fig.1.) was fixed in such a way that r~20a.

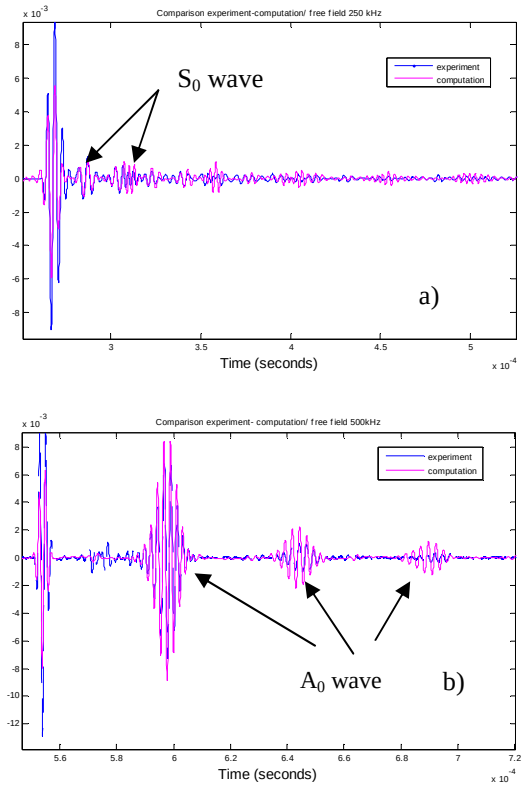

Fig. 4 Echoes of the shell in free space received by: a) transducer T1, b) transducer T2; r ~20a

4 Full field computation

We computed the scattered field for a spherical shell situated 1mm beneath the air-water interface. The calculation was performed for two angles of illumination in the range $0<k_0a<60$. From the scattered field expression

$$\tilde{\Phi}_{scatterer} = -\frac{i}{k_0}\sum_{l=0}^{l_{max}}\sum_{m=0}^{l} A_{ml}(\vec{r})\,T_l\,c_{ml} \qquad (13)$$

we find the form function

$$\left|F_{scatterer}(\omega)\right| = \frac{8\pi r^2}{a}\left|\tilde{\Phi}_{scatterer}(\omega)\right|. \qquad (14)$$

We computed also an approximation of the full scattered field by using the following assumption:

$$c_{ml} = A_{ml}(\vec{r}). \qquad (15)$$

In this case the scattered field can be calculated according the relation:

$$\tilde{\Phi}_{scatterer} = -\frac{i}{k_0}\sum_{l=0}^{l_{max}}\sum_{m=0}^{l}\left(A_{ml}(\vec{r})\right)^2 T_l\,. \qquad (16)$$

The results of these computations are given in Figs. 5 and 6 for the angle of incidence alpha=30°. Fig. 6 is a zoom of Fig. 5 corresponding to the range $0<k_0a<5$.

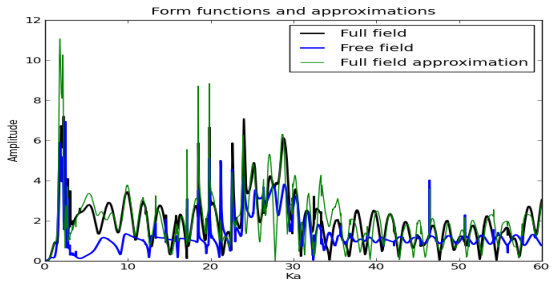

Fig. 5 Computation of the form function for a shell placed 1mm beneath the interface, alpha =30°

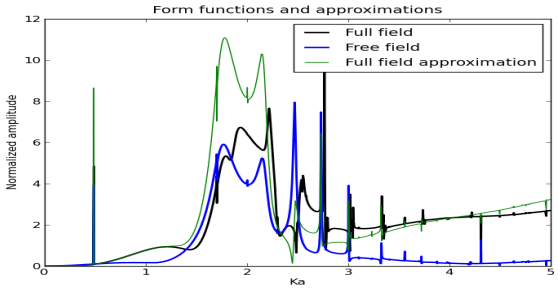

Fig. 6 Zoom of the previous form function in the domain $0<k_0a<5$

In Figs. 5 and 6 it is clearly seen that the frequency response of an object close to an interface is very different from the scattered field of the same object in free field conditions. Arising differences are due to different sort of interactions between the object and interface and between sound wave and interface. These effects depend strongly on both frequency and angle of incidence. They depend also on the distance between sphere and interface. If this distance tends to infinity, there are no more interactions with the interface and the scattered field is just the free field of the object. In Figs. 5 and 6 we give also the results of an approximation of the full field (green curve). This approximation defined by Eq.(15) seems to be relatively acceptable for alpha =30°, but its domain of validity should be studied in details in the future. In Fig. 6 it can be noted that there is a clear shift of the low frequency resonances associated with the antisymmetric Lamb wave when the object is close to the interface. This shift of resonances was already mentioned by R. Lim and al. [5].

4.1 Comparison theory-experiment

In order to check the full field computation, an experiment was carried out in the tank with the same spherical shell as before. The shell was placed beneath the air-water interface being very close to this interface. Different depths of immersion and different angles of incidence were successively studied. Moreover, in order to study the influence of strong resonances of the shell, two wide band Panametrics transducers, working respectively at 250 kHz and 500 kHz were used. A comparison between the experiment and theory can be observed in Fig. 8 for transducer T2 (500 kHz). This transducer is working in the frequency domain corresponding to strong resonances of the object. The echoes obtained for two different angles of incidence (Figs. 7a and 7b) have a very complex structure resulting from strong interactions between interface and object. If we compare modelling and experiment, the general agreement is quite good. In particular, the position of different components of the echoes is well predicted by modelling but as before, small differences in signal amplitude can still be observed.

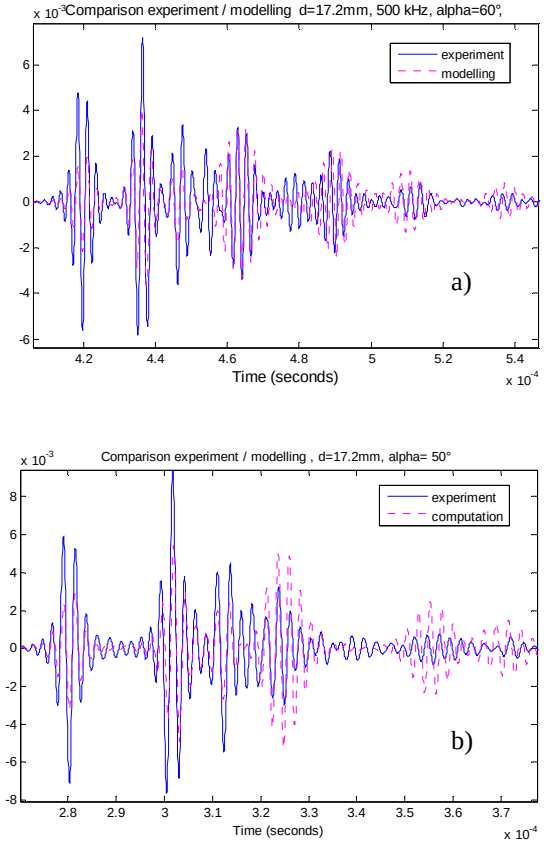

Fig. 7 Echoes of the shell close to the air-water interface: a) α =60°; b) α =50°

Frequency: 500 kHz, r/a~20

In the case of transducer T1 (250 kHz), the frequency range covered by this transducer does not allow excitation of strong resonances. Figure 8 shows an example of echo for the incidence angle of 50°. This signal has a simpler structure than it is shown in Fig. 7b. If we compare modelling and experiment, the general agreement is again satisfactory. In particular, the position of different components of the echoes is well predicted by modelling.

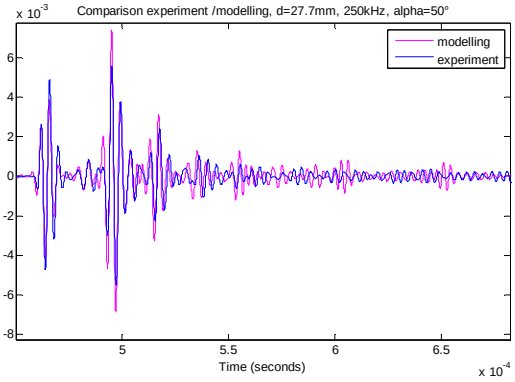

Fig. 8 Echo of the shell close to the air-water interface, α =50°, Frequency: 250 kHz, r/a~20

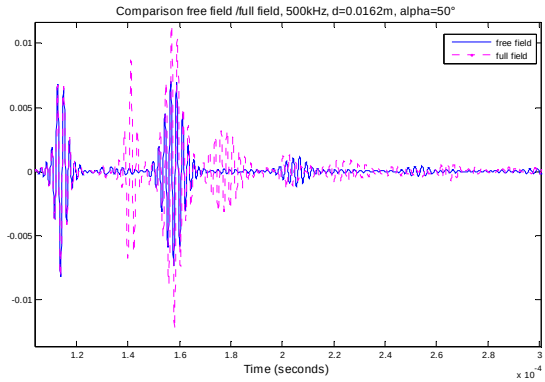

Fig. 10 Comparison free field / full field, transducer T1 (500 kHz)

5 Discussion of the results

5.1 Comparison between a free field echo and an echo with interface interactions

This comparison has been made for transducers T1 and T2. Figure 9 gives the result of comparison for transducer T1 (250 kHz). The two curves have been obtained from experimental data. We can observe that the presence of the air-water interface modifies significantly the structure of the free field echo. This modification of the echo by the environment becomes even more important in the case where strong resonances of the object are excited by transducer T2 (500 kHz). This case is shown in Fig. 10.

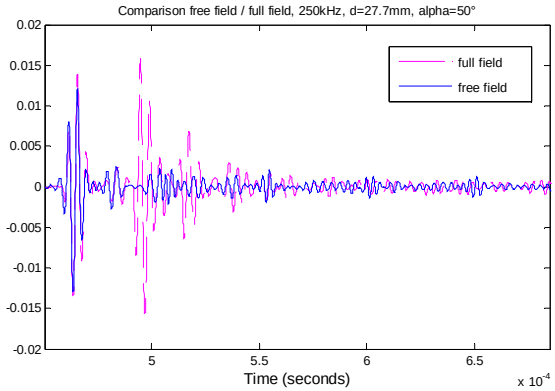

Fig. 9 Comparison free field / full field, transducer T1 (250 kHz)

5.2 Geometrical interpretation of arrivals

In order to understand the structure of the echoes in the situation where the object is close to an interface, and in the most complex situation corresponding to the case, where A_0 waves were excited, we used the ray theory. This simple approach can be used to predict the arrival times of signal components due to direct reflections by the object, successive reflections by interface and object, surface waves of the A_0 type after different circumnavigations on the shell surface, different reflections of these surface waves on the air-water interface.

Seven different paths were used for the computation of travel times are shown in Fig. 11. They include purely geometrical rays and different combinations of surface waves and geometrical rays.

The results of these computations are shown in Fig. 12. We can see a good agreement between the arrival times predicted by the ray theory and different components of the signal which have been clearly identified.

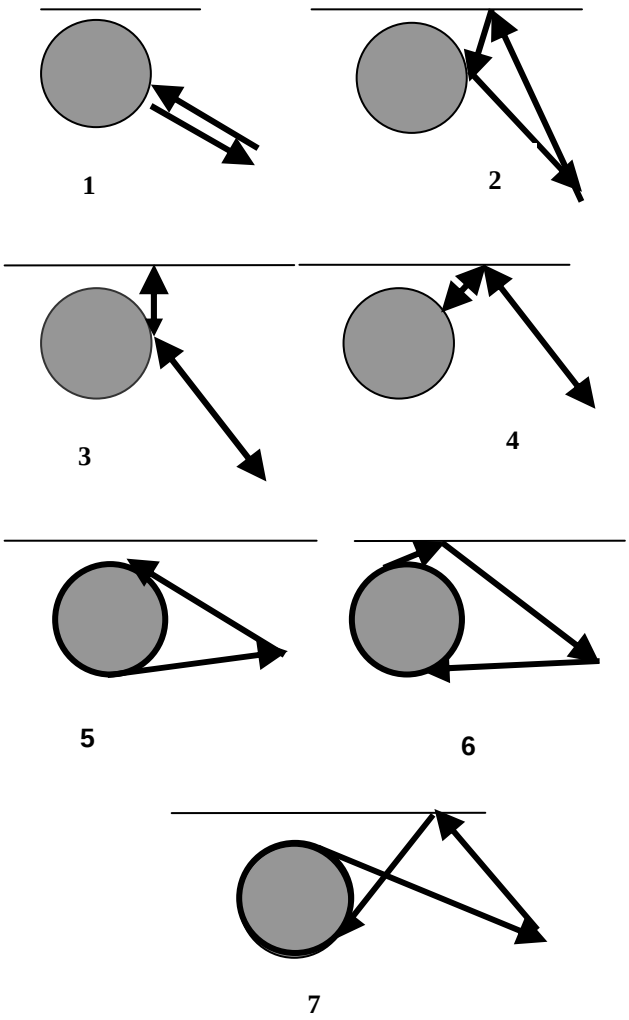

Fig. 11 Rays paths used for calculation of different travel times

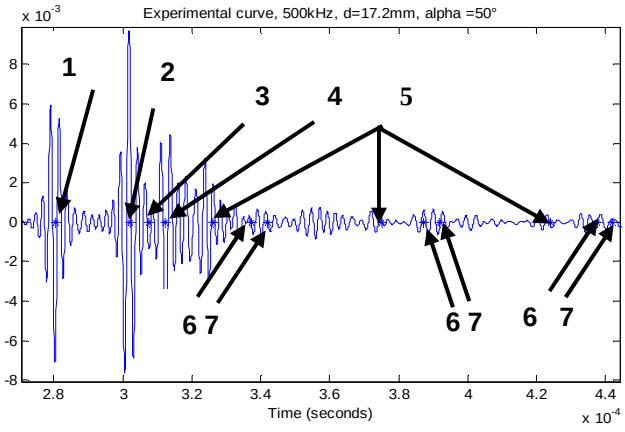

Fig. 12 Arrival times of different components of a signal calculated by the ray theory

6 Conclusion

The results obtained in the present paper confirm the strong influence of the air-water interface on the scattering by an elastic shell placed just beneath this perfectly reflecting interface. This influence depends on several parameters; among them the distance between an object and boundary, the angle of incidence and the frequency content of the transmitted signal. It was shown that in the resonance regimes of the elastic shell, strong interactions due to surface waves can take place and in these conditions it becomes very difficult to identify the target in the time domain. All obtained results were confirmed by tank experiments performed in well controlled conditions. Moreover, we showed that even in a complex case where there are a lot of interactions, the arrival times of different components of the echoes can be predicted by the ray theory.

It should be noted that these results can be extended without too many modifications to the case of an object close to a water-fluid bottom interface.

References

[1] H. Huang and G.C Gaunaurd, "Acoustic point source scattering by a spherical elastic shell submerged beneath a free surface", *J. Acoust. Soc. Am*. 99, 2720-2726 (1996).

[2] R.H Hackman and G.S Sammelmann, "Multiple-scattering analysis for a target in an oceanic waveguide", *J. Acoust. Soc. Am*. 84, 1813-1825 (1988).

[3] J.A. Fawcett and R. Lim, "Evaluation of the integrals of target/seabed scattering using the method of complex images", *J. Acoust. Soc. Am*. 114, 1406-1415 (2003).

[4] S.G. Kargl and P.L. Marston, "Ray synthesis of Lamb wave contributions to the total scattering cross section for an elastic spherical shell," *J. Acoust. Soc. Am*. 88, 1103-1113 (1990).

[5] R. Lim, J.L. Lopes, R.H Hackman, and D.G. Todoroff, "Scattering by objects buried in underwater sediments: Theory and experiments", *J. Acoust. Soc. Am*. 93, 1762-1783 (1993).

[6] G.C. Gaunaurd and H. Huang, "Acoustic scattering by a spherical body near a plane boundary", *J. Acoust. Soc. Am*. 96, 2526-2536 (1994).

[7] A. Messiah, "Clebsch-Gordan (C.G.) coefficients and 3j symbols," Appendix C.I in *Quantum Mechanics*, Vol 2, 1054-1060, North-Holland, Amsterdam, The Netherlands, (1962).

[8] J.D. Murphy, J. George, A. Nagl and H. Überall, "Isolation of the resonance component in acoustic scattering from fluid loaded elastic spherical shells", *J. Acoust. Soc. Am*. 65, 368-373 (1979)

[9] G.S.Sammelmann, D.H. Trivett, and R.H. Hackman, “The acoustic scattering by a submerged, spherical shell, I: The bifurcation of the dispersion curve for the spherical antisymmetric Lamb wave”, *J. Acoust. Soc. Am.* 85, 114-124 (1989)

[10] J-P Sessarego, J. Sageloli, C. Gazanhes and H. Überall, “Two Scholte –Stoneley waves on doubly fluid-loaded plates and shells”, *J. Acoust. Soc. Am*. 101(1), 135-142 (1997)

[11] M Zakharia, F. Magand, J.-P. Sessarego, J. Sageloli, “Application of time frequency analysis to the characterization of acoustical scattering”, published in “Acoustical Interactions with Submerged Elastic Structures”, Part III, pp. 168-204, Ed by A. Guran, A. De Hoop and F. Mainardi, Series on Stability, Vibration and Control of Systems, Series B: Vol 5, World Scientific Publishing Company, (2002).